International Journal of Heat and Mass Transfer 173 (2021) 121207

Contents lists available at ScienceDirect

International Journal of Heat and Mass Transfer

journal homepage: www.elsevier.com/locate/hmt

Pressure-dependent weighted-sum-of-gray-gases models for heterogeneous CO_2-H_2O mixtures at sub- and super-atmospheric pressure

Hadi Bordbar[a,*], Felipe R. Coelho[b], Guilherme C. Fraga[b], Francis H.R. França[b], Simo Hostikka[a]

[a] Department of Civil Engineering, Aalto University, Rakentajanaukio 4a, Espoo, 02150, Finland
[b] Mechanical Engineering Department, Universidade Federal do Rio Grande do Sul, Porto Alegre, RS, Brazil

ARTICLE INFO

Article history:
Received 8 December 2020
Revised 23 February 2021
Accepted 7 March 2021
Available online 31 March 2021

Keywords:
Weighted-sum-of-gray-gases model (WSGG)
Thermal radiation
Pressurized combustion
Spectral radiation
Sub-atmospheric combustion

ABSTRACT

The effect of total pressure of gas mixture is included in the development of new coefficients for the weighted-sum-of-gray-gases model (WSGG). The WSGG formulation previously reported by Bordbar et al. (combustion and Flame 2014, V. 161, pp. 2435–2445), which accounts for variations of molar fraction ratio of H_2O to CO_2, was employed here to obtain a new total pressure-dependent WSGG model. Hence, the new model includes both the effect of total pressure and variation of molar fraction ratio. High-resolution absorption spectra of gases produced by line-by-line (LBL) calculations using the HITEMP2010 spectral database are used to produce the total emissivity databases needed for the WSGG model development and also to produce the benchmark solution of one-dimensional slab problems used for validation of the new model. The performance of the new WSGG model is studied through several test cases representing various conditions of total pressure, inhomogeneity of temperature, concentration of gas species and molar fraction ratios. In all cases, the new model exhibits a good agreement with the LBL solutions. The new WSGG coefficients allow the model to efficiently solve the spectral thermal radiation in both sub- and super-atmospheric combustion systems.

1. Introduction

With recent increment in computational resources, the role of numerical modeling in design process of energy conversion systems has more and more highlighted [1,2]. With an increasing trend during the last three decades, numerical modeling exhibited promising capability to analyze various physical phenomena occurring in energy conversion systems including the pollutants emission [3], multi-phase flow [4–6], turbulence [7,8] and thermal radiation [9–11].

Thermal radiation is the major heat transfer mode in combustion processes, due to the high temperatures involved and the presence of species that emit and absorb radiative energy, such as carbon dioxide, water vapor and soot [2,3,12,13]. The determination of the radiation field entails the solution of the radiative transfer equation (RTE), which is an integro-differential equation in space and in two directional coordinates with local origin [14,15]. Moreover, the radiative properties (in particular, the absorption coefficient) of diatomic and polyatomic molecules present a complex dependence on the radiation spectrum, often characterized by hundred of thousands to millions of spectral lines, whose positions and intensity are in turn dependent on the local thermodynamic state [10]. To obtain the total radiation intensity and related quantities (e.g., the radiative heat flux and the volumetric radiative heat source), the RTE needs to be additionally integrated over the entire spectrum, which, for species as CO_2 and H_2O, introduces another formidable level of difficulty to the problem.

While radiation modeling of air-fuel combustion at atmospheric conditions is already a challenging task, it can be further complicated for oxy-fuel combustion and for high-pressure conditions. In the former, the possibility of large variations in the chemical concentration of the participating species and its effect on the radiation absorption spectrum need to be accounted for. This can be particularly significant for species such as H_2O, whose absorption spectrum presents a non-negligible self-broadening effect [16]. The total pressure also affects, even more substantially than changes in mole fraction, the absorption spectra of all participating species, by

* Corresponding author.
E-mail address: hadi.bordbar@aalto.fi (H. Bordbar).

https://doi.org/10.1016/j.ijheatmasstransfer.2021.121207

increasing the values of the absorption coefficient and smoothing its highly-irregular spectral variation [17,18].

The aforementioned complex spectral dependence of the absorption coefficient of some species can be captured with a high degree of accuracy in the integration of the spectral radiation intensity by the line-by-line (LBL) methodology. In the LBL calculations, detailed information of the absorption lines is extracted from high-resolution spectral databases, so as to allow each one of them to be individually considered. However, the need of solving the RTE many thousands of times for each optical path makes the computational cost of the LBL methodology prohibitive for most applications [11]. This justifies the rise and broad use of models to represent the wavenumber dependence of the radiative transfer is an approximate and less computationally-intensive manner.

Recent years have seen much effort invested in developing or adapting existing spectral models for applications outside of air-fuel, and atmospheric combustion. Narrow-band models—and, particularly, the statistical narrow-band (SNB) model [19,20]—have been successfully applied for oxy-fuel combustion at high-pressure conditions (as in, e.g., [21]), with results showing errors of about 2% relative to the LBL solution for total pressures as high as $p = 30$ *atm*. The SNB correlated-*k* distribution (SNBCK) model, which is based on a reordering the spectral absorption coefficient of each narrow-band into a monotonically increasing function in order to simplify and reduce the computational cost of the traditional SNB model, was also found to be accurate for both oxy-fuel and high-pressure combustion. For instance, Kez et al. [22] carried out the first analysis of the SNBCK model for three-dimensional cases representative of high-pressure (20 *atm*), oxy-fuel combustion problems; using the SNB model as the reference, the errors of the SNBCK solution were of at most 2.5%. Additional tests of the SNBCK model in similar conditions are reported in [21,23,24].

Wang and Modest [25] developed a new narrow-band *k*-distribution database for CO_2 and H_2O for total pressures ranging from 0.1 to 30 *bar*, based on which narrow-band and full-spectrum *k*-distributions can be obtained for non-homogeneous mixtures. Using this database, the full-spectrum *k*-distribution (FSK) model was applied [26] to predict the radiative heat source in two-dimensional, homogeneous CO_2-H_2O mixtures at a total pressure of 30 *atm*, with maximum errors relative to the LBL solution of 11%. Although the medium composition in [26] was inline with characteristic of air-fuel combustion, subsequent studies showed that the FSK model is capable of providing accurate solutions for both atmospheric [27–29] and high-pressure oxy-fuel combustion scenarios [21–24]. Following the work of [25], the narrow-band *k*-distribution database was updated in [30] by employing more complete spectroscopic data and expanding it to a wider range of pressures.

The absorption-line blackbody distribution function (ALBDF), necessary for the application of the spectral line-based weighted-sum-of-gray-gases (SLW) model [31,32], has also recently been updated for the full mole fraction range for CO_2, H_2O and CO for total pressures between 0.1 *atm* and 50 *atm* [33,34]. Chu et al. [23] also applied the SLW model to a set of high-pressure, oxy-fuel problems, finding an accuracy comparable to the FSK model as long as a sufficient number of gray gases is used. Furthermore, because [23] did not use the most up-to-date ALBDFs of [33,34], it is possible that the performance of the SLW is even better.

In contrast to all these models, the weighted-sum-of-gray-gases (WSGG) model has yet to be consolidated for the treatment of high-pressure conditions. This model is based on a similar principle as the FSK and SLW models. However, because it presents a simpler formulation and smaller computational data and costs, it likely is the most widely used global spectral model for combustion applications. The literature reports various well-established WSGG correlations for mixtures representative of air-fuel and oxy-fuel combustion at atmospheric pressure (see, e.g., [35–40]), with many studies attesting their accuracy at these conditions [41–44]. However, as it was shown in [21–23], using WSGG correlations developed for atmospheric pressure for high-pressure applications leads to considerable errors.

Hence, attention toward development of WSGG formulations for high-pressure applications has increased in the last decade, and the main studies on the subject are summarized in Table 1. The pioneering work on this field was the one by Bahador and Sunden [45], who developed WSGG correlations for pure H_2O and CO_2-H_2O mixtures at total pressures ranging between 1 *atm* and 20 *atm*. The correlations were generated using an approach that is typical for WSGG model, by fitting total emittance to a reference data, which in [45] were extracted from the HITEMP1995 [46] and CDSD-1000 [47] spectroscopic databases. A similar effort, albeit using the more accurate HITEMP2010 [48] database for the emittance fittings, was undertaken by Coelho and França for pure species [49] and for CO_2-H_2O mixtures characteristic of methane-air combustion [50]. Furthermore, differently from [45], which only presented comparisons of the total emittance, radiative transfer calculations of a set of one-dimensional test cases were carried out in [49,50], with their model showing a good level of agreement to the LBL method.

Shan et al. [51] developed the first WSGG formulation for high-pressure, oxy-fuel combustion scenarios, based on emittance fittings to the EM2C narrow-band model. Following the same approach as some WSGG formulations for atmospheric pressures [36,52], these fittings were constructed for fixed H_2O/CO_2 mole ratios M_r and a stepwise interpolation methodology was devised for dealing with varying-M_r scenarios. Instead of generating WSGG coefficients for discrete total pressure values as the aforementioned papers did, Shan et al. [51] let the coefficients be dependent on total pressure itself, within a range $1\ bar \leq p \leq 30\ bar$. A similar model was introduced by Wang and Xuan [35] for aircraft engine applications, considering the same total pressure range, but only for a single M_r. Both [51] and [35] report good accuracy of their respective models in one-dimensional radiative transfer calculations.

The present study proposes a new WSGG formulation for CO_2-H_2O mixtures representative of high-pressure combustion. This is a direct extension of the WSGG correlation for atmospheric pressure previously reported by Bordbar et al. [40] to other values of total pressure (p), and, as depicted in Table 1, it covers a wider range of total pressures, moleratios and temperatures than the WSGG formulation of Shan et al. [51]. Moreover, the new model is based on the HITEMP2010 [48] spectral database, which is more accurate than the EM2C narrow-band model used as a reference in that paper. Also, by incorporating the M_r dependence into the WSGG coefficients (rather than generating coefficients for discrete moleratio values, as in [51]), it provides a more convenient treatment of problems where M_r varies throughout the domain.

Besides high-pressures, the pressure range of the formulation developed here also includes sub-atmospheric conditions (as low as 0.1 *atm*). While radiative transfer calculations at these conditions are rare outside of meteorological applications [14], sub-atmospheric pressures have often been used as a surrogate to study microgravity combustion (for example, [53–55]), so an accurate treatment of radiation at these low pressures may prove to be important. However, spectral modeling at sub-atmospheric pressures is still a fairly unexplored subject of study, and, as far as the authors' know, this is the first WSGG model that contemplates these conditions.

2. Model development

To obtain the emissivity database needed for development of new pressure-dependent WSGG model, the line-by-line integration method is implemented to produce the required absorption spec-

Table 1
Summary of the different existing formulations of the WSGG model developed for high-pressure applications.

WSGG formulation	Reference	Species/Mixture	T range	M_r values/range	p values/range
Bahador and Sunden [45]	HITEMP1995, CDSD-1000	H_2O, CO_2-H_2O	500K–2500K	1.0 and 2.0	(1.0; 2.5; 5.0; 7.5; 10; 12.5; 15; 20) *atm*
Coelho and França [49]	HITEMP2010	CO_2, H_2O	400K–2500K	–	(1.0; 10; 40) *atm*
Coelho and França [50]	HITEMP2010	CO_2-H_2O	400K–2500K	2.0	(1.0; 2.0; 5.0; 10; 20; 40) *atm*
Shan et al. [51]	EM2C	CO_2-H_2O	500K–2500K	0.125–4.0	1bar–30bar
Wang and Xuan [35]	HITEMP2010	CO_2-H_2O	500K–2500K	1.0	1 *atm*–30 *atm*
Present paper	HITEMP2010	CO_2-H_2O	300K–3000K	0.1–4.0	(0.1; 0.5; 1.0; 2.0; 10; 20; 30; 50; 80) *atm*

tra of the gases by using the HITEMP2010 spectral database [48]. The details of the line-by-line calculation of the absorption spectra of gas mixtures is well described in the literature (see, for instance, [10,39,40,50]). However, for the sake of completeness, this section first briefly reviews the line-by-line calculations and its characteristics in the present research, and then explains how they are used for development of the new WSGG model.

2.1. Determination of the line-by-line based emissivity database

The spectral absorption coefficient of CO_2 and H_2O in each spectral segment depends on the wavenumber, temperature, the partial pressure of the gases and the total pressure of the gas mixture. The properties of a spectral line i of CO_2 and H_2O including the line intensity S_i, the line center wavenumber ν_i, the Lorentz broadening half-width γ_L, and the Doppler broadening half-width γ_D, can all be obtained or calculated from spectral databases, i.e. HITEMP2010 [48]. In the present work, depending on the relative importance of Doppler broadening to Lorentz broadening, two different line profiles, Lorentz and Voigt, have been implemented in the line by line calculation of absorption spectra of combustion gases. The theory of calculating spectral absorption coefficient along the lines by these two line profiles are described below.

Assuming the combined effect of natural line broadening and collision broadening, the Lorentz line profile evaluates the absorption coefficient at an arbitrary wavenumber ν from a particular spectral line with line center at ν_i as

$$\kappa_{\nu,i} = \frac{S_i}{\pi} N(p,T) \frac{\gamma_{L,i}}{\gamma_{L,i}^2 + (\nu - \nu_i)^2}, \tag{1}$$

where $\kappa_{\nu,i}$ is the absorption coefficient for the i^{th} spectral line at the wavenumber location ν, S_i is the molecule-based intensity of the i^{th} spectral line, $N(p,T)$ is the number density, $\gamma_{L,i}$ is the Lorentz broadening half width of this spectral line, and ν_i is the spectral line location. Applying the ideal gas assumption, the number density is calculated as $\frac{N_A}{RT} p Y_g$ where N_A, R, Y_g, p and T represent the Avogadro's number, the gas constant, the gas mole fraction, pressure and temperature, respectively. The temperature-dependent intensity of each spectral Lorentz line is given as

$$S_i = S_i(T_{ref}) \frac{Q(T_{ref})}{Q(T)} \frac{\exp(-hcE_{\nu_i}/kT)}{\exp(-hcE_{\nu_i}/kT_{ref})} \frac{[1-\exp(-hc\nu_i/kT)]}{[1-\exp(-hc\nu_i/kT_{ref})]}, \tag{2}$$

where Q is internal partition function of the molecule at temperatures T and T_{ref}, E_ν is the lower-state energy of the line, c is the speed of light in vacuum, and k and h are the Boltzmann and Planck constants, respectively. A reference temperature of $T_{ref} = 296K$ is set for the present LBL calculations. The collision broadening of the spectral line depends on temperature, partial pressure and total pressure as

$$\gamma_{L,i} = \left(\frac{T_{ref}}{T}\right)^n [\gamma_{air}(p - p_s) + \gamma_{self} p_s], \tag{3}$$

where γ_{air} and γ_{self} are the line air- and self-broadening, respectively, n is the temperature-dependence coefficient, and p_s is the partial pressure of the species.

The spectral-line profile to produce the histograms for each line is defined based on the relative importance of the Lorentz to Doppler line-broadening effects. Using narrow-band transmissivities as a comparion criterion, Wang and Modest [17] reported that at low pressures (< 1 *bar*) and high temperatures ($> 2500K$), the Doppler broadening may become an important mechanism and therefore the combined Lorentz-Doppler line profile (or Voigt) should be used. In contrast to the Lorentz profile, the Voigt profile does not have a closed form and is instead given as

$$\kappa_{\nu,i} = \frac{S_i \gamma_{L,i}}{\pi^{1.5}} N(p,T) \int_{-\infty}^{+\infty} \frac{\exp(-x^2)}{[\nu - \nu_i - x\gamma_{D,i}(\ln 2)^{-0.5}]^2 + {\gamma_{L,i}}^2} \mathrm{d}x \tag{4}$$

The Humleek algorithm [56] as given in [14] is used to calculate the Voigt profile in the present work whenever needed. Because, in general, the Voigt profile is recommended when the Doppler line half-width γ_D is comparable to the Lorentz half-width γ_L [14], the criterion $\gamma_L/\gamma_D < 10$ is adopted for selecting the Voigt profile, with the Lorentz profile being used otherwise. A minimum limit of absorption coefficient equals $^{10^{-9}}$ cm^{-1} is considered as the cut off limit of the line wings.

In order to calculate the absorption coefficient for an arbitrary wavenumber, the contribution of all significant neighboring lines needs to be taken into account. This is done by simply summing up all the contributions of the spectral lines at wavenumber ν,

$$\kappa_\nu = \sum_i \kappa_{\nu,i} \tag{5}$$

In this work, the line by line absorption spectra of two gases are obtained for the range of 150 cm^{-1} to 25000 cm^{-1}. This spectral range is much wider than the one used in development of the atmospheric WSGG model of Bordbar [40] and is wide enough to include the emission power of high temperatures. It for instance accounts for 99.8% of the total balckbody emissive power at 3000 K [33].

For the sub-atmospheric pressures, a fine resolution of $0.005cm^{-1}$ is needed to produce accurate absorption spectra of gases. Further refinement beyond this limit has been reported to have negligible effect [33]. It yields to 4,970,000 evenly spaced spectral intervals of 0.005 cm^{-1} between 150 cm^{-1} and 25000 cm^{-1}.

For atmospheric and higher pressures, the resolution of 0.01 cm^{-1} is used to obtain the absorption spectra of gases. It is fine enough for these pressures and using higher spectral resolutions has a negligible influence on the results while causing a great increment to the computational cost as shown in the previous reports[57,58]. It yields to 2,485,000 evenly spaced spectral intervals of 0.01 cm^{-1} between 150 cm^{-1} and 25000 cm^{-1}.

The spectral-line location, intensity, and air and self-broadening are taken from the spectroscopic database HITEMP2010 [48]. For the present work, the profiles of linear spectral absorption coefficient of H_2O and CO_2 were obtained considering various total pressures, molar fraction ratios and temperatures needed for the

WSGG model development. This was done for ten different total pressures (0.1, 0.5, 1.0, 2.0, 5.0, 10.0, 20.0, 30.0, 50.0, and 80.0 *atm*) and at fifty-five evenly-spaced temperature values between 300K and 3000 K—i.e., with a step of 50 *K*. For each total pressure and temperature, thirty-three discrete values of the mole fraction ratio were considered, M_r = 0.1, 0.125, 0.25 0.375, 0.5, 0.625, 0.75, 0.875, 1.0, 1.125, 1.25, 1.375, 1.5, 1.625, 1.75, 1.875, 2.0, 2.125, 2.25, 2.375, 2.5, 2.625, 2.75, 2.875, 3.0, 3.125, 3.25, 3.375, 3.5, 3.625, 3.75, 3.875, and 4.0. From these values, the mole fractions of H_2O and CO_2 (and, consequently, their partial pressures) were calculated by assuming that the gas mixture contains only these two species, following [40]. Hence, the mole fraction of CO_2 is obtained as $Y_{CO_2} = 1/(1+M_r)$, and the mole fraction of H_2O, as $Y_{H_2O} = 1 - Y_{CO_2}$. Although this corresponds to oxygen-fired combustion products, the WSGG model generated from these parameters can be safely applied to air-fired combustion scenarios as well, as demonstrated in [59] for the atmospheric-pressure WSGG model of [40], which was generated following a similar methodology. The linear absorption spectra of individual gases at each mixture (i.e. represented by a total pressure, a molar fraction ratio and a temperature) were then used to calculate the emissivity of the gas mixtures needed for development of the new pressure dependent WSGG model.

The emissivity of the gas mixture, which is used as the curve-fitting parameters for determining the coefficients of the WSGG model (cf. Section 2.2) at each pressure, mole fraction ratio and temperature is calculated as

$$\varepsilon = \frac{1}{I_b}\int_0^\infty I_{b\nu}\{1-\exp[-(\kappa_{\nu,H_2O}+\kappa_{\nu,CO_2})L]\}\mathrm{d}\nu \tag{6}$$

where $I_{b\nu}$ and I_b are the spectral and total blackbody radiation intensity, respectively ($I_b = \int_0^\infty I_{b\nu}\mathrm{d}\nu$), κ_{ν,H_2O} and κ_{ν,CO_2} are the absorption coefficient of water vapor and carbon dioxide, respectively, and L is the path length. For generating the WSGG model, the emissivity is computed for nineteen different path lengths, L = 0.01, 0.05, 0.1, 0.2, 0.3, 0.4, 0.5, 0.75, 1.0, 1.5, 2.0, 3.0, 5.0, 10.0, 15.0, 20.0, 30.0, 45.0, and 60.0 *m*. This, combined to the fifty-five discrete temperature values and thirty-three discrete mole ratio values, yields a LBL-based emissivity database with 34485 points for each one of the ten aforementioned total pressures.

2.2. Development of pressure-dependent WSGG model

The WSGG model is a non-gray global spectral model that replaces the absorption spectrum of a given species or mixture by a set of gray gases and a transparent window. Each gray gas i has an absorption coefficient κ_i (that does not vary with ν) and covers a fixed although not necessarily continuous, portion $\Delta\nu_i$ of the radiation spectrum. From these considerations, the integration over the spectrum in Eq. (6) becomes [60]

$$\varepsilon = \sum_{i=1}^{N_g} a_i\{1-\exp[-\kappa_{p,i}(p_{H_2O}+p_{CO_2})L]\}, \tag{7}$$

where N_g, a_i and $\kappa_{p,i}$ is the number of gray gases, the weighting factor of each gray gas and its pressure-based absorption coefficient, respectively, and p_{H_2O} and p_{CO_2} are the partial pressures of H_2O and CO_2. A total of four gray gases ($N_g = 4$) is adopted for the present model, with an additional transparent window denoted as $i = 0$. Using larger number of gray gases only marginally improve the accuracy of the model while increasing the CPU cost of RTE solution significantly.

The weighting factors a_i in Eq. (7) represent the fraction of blackbody energy that lies within $\Delta\nu_i$. Here, they are described as a fourth order polynomial of the normalized temperature $\hat{T} = T/1500K$,

$$a_i = \sum_{j=0}^{4} b_{ij}\hat{T}^j, \qquad (i = 1,\ldots,4), \tag{8}$$

where b_{ij} is the j^{th} degree polynomial coefficient of gas i. Using a normalized temperature instead of the temperature itself in the above equation facilitates the fitting process and is an approach often adopted in the literature (e.g., [3,37,41,51]). The weighting factor of the transparent window, on the other hand is defined as to satisfy the energy conservation principle,

$$a_0 = 1 - \sum_{i=1}^{N_g} a_i. \tag{9}$$

For each molar fraction ratio at each total pressure value, the b_{ij} and $\kappa_{p,i}$ are found by fitting Eq. (7) to the LBL emissivity database across the discrete values of T and L defined in Section 2.1. The fitting is done with the `lsqcurvefit` function of MATLAB R2019b, which is a nonlinear least-squares solver as described in [61]. Afterwards, following [40], the effect of molar fraction ratio in a single set of WSGG model coefficients for each total pressure is included by expressing b_{ij} and $\kappa_{p,i}$ as

$$b_{ij} = \sum_{k=0}^{4} c_{ijk}M_r^{(4-k)}, \tag{10}$$

$$\kappa_{p,i} = \sum_{k=0}^{4} d_{ik}M_r^{(4-k)}, \tag{11}$$

in which c_{ijk} and d_{ik} are the constants of the model. For each of the ten total pressures considered here, a different set of constants is obtained. To ease the implementation of the present model, the coefficients of the new WSGG models are given in the supplementary materials of this paper, alongside a simple MATLAB function to implement the model.

3. The WSGG model and the radiative transfer equation

For participating, non-scattering media, the spectral radiative transfer equation (RTE) is given by [14,16]

$$\frac{dI_\nu}{ds} = -\kappa_\nu I_\nu + \kappa_\nu I_{b\nu}, \tag{12}$$

where I_ν is the local spectral radiation intensity, κ_ν is the spectral absorption coefficient (for a H_2O-CO_2 mixture, $\kappa_\nu = \kappa_{\nu,H_2O} + \kappa_{\nu,CO_2}$), and s is the coordinate along the path of radiation propagation. The global solution of the radiative heat transfer entails the integration of the above equation over the spectrum and across all directions. Applying the WSGG model, the total radiation intensity I in a certain direction is determined as a simple summation of the partial intensities I_i of each gray gas i (and of the transparent window), i.e., $I = \int_0^\infty I_\nu\mathrm{d}\nu = \sum_{i=0}^{N_g} I_i$. The partial intensities I_i are in turn obtained from the integration of Eq. (12) over the region of the spectrum corresponding to the i^{th} gray gas,

$$\frac{dI_i}{ds} = -\kappa_i I_i + a_i\kappa_i I_b. \tag{13}$$

It has been shown in [60] that the WSGG model can be used alongside any method for the spatial integration of the RTE. In the present study, the discrete ordinates method (DOM) is chosen for this purpose, which solves the RTE for a discrete set of directions and computes the continues integral over all solid angles through a quadrature scheme [62,63]. The cases considered here consists of a one-dimensional medium slab as depicted in Figure 1, where the participating medium is bounded by two parallel black walls.

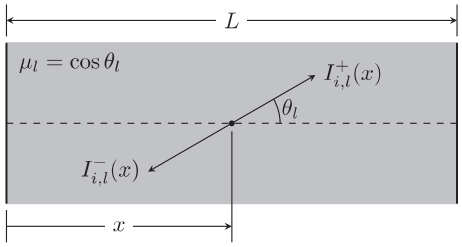

Fig. 1. Schematic representation of the one-dimensional domain for the RTE solution with the WSGG model and the DOM (adapted from [64]).

For this configuration, the DOM determines the partial intensities in the forward and backward directions ($I^+_{i,l}$ and $I^-_{i,l}$, respectively, as also shown in Figure 1) from the solution of the following equations

$$\mu_l \frac{dI^+_{i,l}}{dx} = -\kappa_i I^+_{i,l} + a_i \kappa_i I_b \,, \tag{14}$$

$$-\mu_l \frac{dI^-_{i,l}}{dx} = -\kappa_i I^-_{i,l} + a_i \kappa_i I_b \,, \tag{15}$$

where μ_l is the cosine of the polar angle θ_l in direction l, and x is the spatial position. For black walls with known temperatures, the boundary conditions for these equations are set at the positions $x = 0$ and $x = L$ (with L being the medium length), respectively: $I^+_{i,l}(0) = a_i(0) I_b(0)$ and $I^-_{i,l}(L) = a_i(L) I_b(L)$.

Once Eqs. (14) and (15) have been solved, the total radiative heat flux and the volumetric radiative heat source at position x ($q_r(x)$ and $S_r(x)$, respectively) may be determined as

$$q_r(x) = 2\pi \sum_{i=0}^{N_g} \sum_{l=1}^{N_d} \mu_l \omega_l [I^+_{i,l}(x) - I^-_{i,l}(x)] \,, \tag{16}$$

$$S_r(x) = 2\pi \sum_{i=1}^{N_g} \sum_{l=1}^{N_d} \omega_l \kappa_i(x) \{[I^+_{i,l}(x) + I^-_{i,l}(x)] - 2a_i(x) I_b(x)\} \,, \tag{17}$$

in which N_d is half the total number of discrete directions and ω_l is the quadrature weight associated to direction l. For the calculations in this study, the values of μ_l and ω_l are extracted from the quadrature scheme of Lathrop and Carlson [65], with the weights normalized as to satisfy $\sum_{l=1}^{n_d} \omega_l = 1$.

4. Results

4.1. Emissivity charts

Although the main advantage of the WSGG model is to accurately account for spectral variation of gas mixtures with a reasonable computational cost, the model has been widely used to calculate the effective absorption coefficient used in gray gas modeling—it is, for instance, the base of the main gas radiation property model of Ansys-Fluent [66]. In this kind of gray gas modeling, Beer-Lambert's law is invoked to estimate the effective absorption coefficient from the total emissivity assuming a mean beam length (L) as $\kappa = -\ln(1-\varepsilon)/L$ [16]. The emissivity in this formulation is often determined from three-dimensional charts that present ε as a function of the temperature and the path length for a given total pressure and molar fraction ratio.

To assess the accuracy of the WSGG model developed here for such applications, Figure 2 compares the emissivity computed by applying the new model to Eq. (7) and the emissivity directly obtained by line-by-line integration of Eq. (6) using the absorption spectra extracted from the HITEMP2010 database. For conciseness, only results for typical dry and wet flue gas recycle conditions (i.e., $M_r = 0.125$ and $M_r = 1.0$, respectively) at the smallest and largest pressures considered in this study ($p = 0.1atm$ and $p = 80atm$) are reported in that figure.

For all the cases and across most of the temperature range of $300K \le T \le 3000K$, the total emissivities calculated by the present WSGG model are in a good agreement with those determined by the LBL method. However, larger discrepancies are seen at low temperatures in $p = 0.1$ atm, especially for larger path lengths. At this pressure, the emissivity as obtained by the LBL method changes more strongly with temperature for $T < 1000K$ than anywhere else in the charts particularly for larger lengths. In these low temperatures, the emissivity first decreases with temperature (300K - 500K), and then increases with temperature until $T = 1000$K. The emissivity then decreases with temperature for all the higher temperatures. The larger discrepancies between the emissivity predicted by the WSGG model and LBL method occurring at lower temperatures are explained by the inability of the WSGG model in reproducing the abrupt change of the LBL emissivity. Conversely, for $p = 80atm$, the LBL emissivity is less affected by changes of temperature at lower temperatures, and therefore the WSGG model (Eq. (7)) can more accurately reproduce the emissivities calculated by the LBL method.

4.2. Benchmark cases

Three test cases are considered to evaluate the performance of the new WSGG model, consisting of one-dimensional radiative transfer calculations for the domain depicted in Figure 1, with a medium length $L = 1m$. The temperature profile for all cases is the same, given as

$$T(\hat{x}) = 300K + 1500K \sin^2(\pi \hat{x}) \,, \tag{18}$$

where $\hat{x} = x/L$, with x denoting the distance from the left wall (cf. Figure 1). This is a symmetrical profile, with $T = 300K$ at the walls and a maximum temperature of $1800K$ at the center of the medium (note though that the WSGG model proposed in this paper is applicable for temperatures as high as 3000 K); similar T-distributions have been previously applied for assessing other WSGG models, e.g., [39,44,50,67].

The test cases differ between one another by the concentration of the medium, for which three (also symmetrical) profiles are tested, defined by the following mole fraction expressions for H_2O and CO_2 (Y_{H_2O} and Y_{CO_2}, respectively):

$$\text{Case 1:} \quad Y_{H_2O}(\hat{x}) = 0.2 \sin^2(\pi \hat{x}) \,, \qquad Y_{CO_2} = Y_{H_2O}/2 \,; \tag{19}$$

$$\text{Case 2:} \quad Y_{H_2O}(\hat{x}) = 0.1\left[1 + sin^2(\pi \hat{x})\right] \,, \quad Y_{CO_2} = 1 - X_{H_2O} \,; \tag{20}$$

$$\text{Case 3:} \quad Y_{H_2O}(\hat{x}) = \frac{1}{3}\left[1 + \sin^2(\pi \hat{x})\right] \,, \quad Y_{CO_2} = 1 - X_{H_2O} \,. \tag{21}$$

Eq. (19) illustrates a scenario of air-fuel combustion with $M_r = 2$, characteristic of the stoichiometric combustion of methane (for this profile, the remainder of the mixture is assumed to be composed of a transparent gas). Eq. (20), (21) represent oxy-fuel combustion conditions: the former, with dry flue gas recirculation, where the mole ratio varies between 1/9 and 1/4; and the latter, with wet-flue gas recirculation, in which $0.5 \le M_r \le 2.0$.

The solution of the RTE through the discrete ordinates method, as described in Section 3, is carried out numerically by a finite differencing approach. The medium is discretized in a total 200 grid cells and the number of discrete ordinates for the application of the DOM is set to twelve; further spatial and directional refinements did not significantly impact the results. The reference for

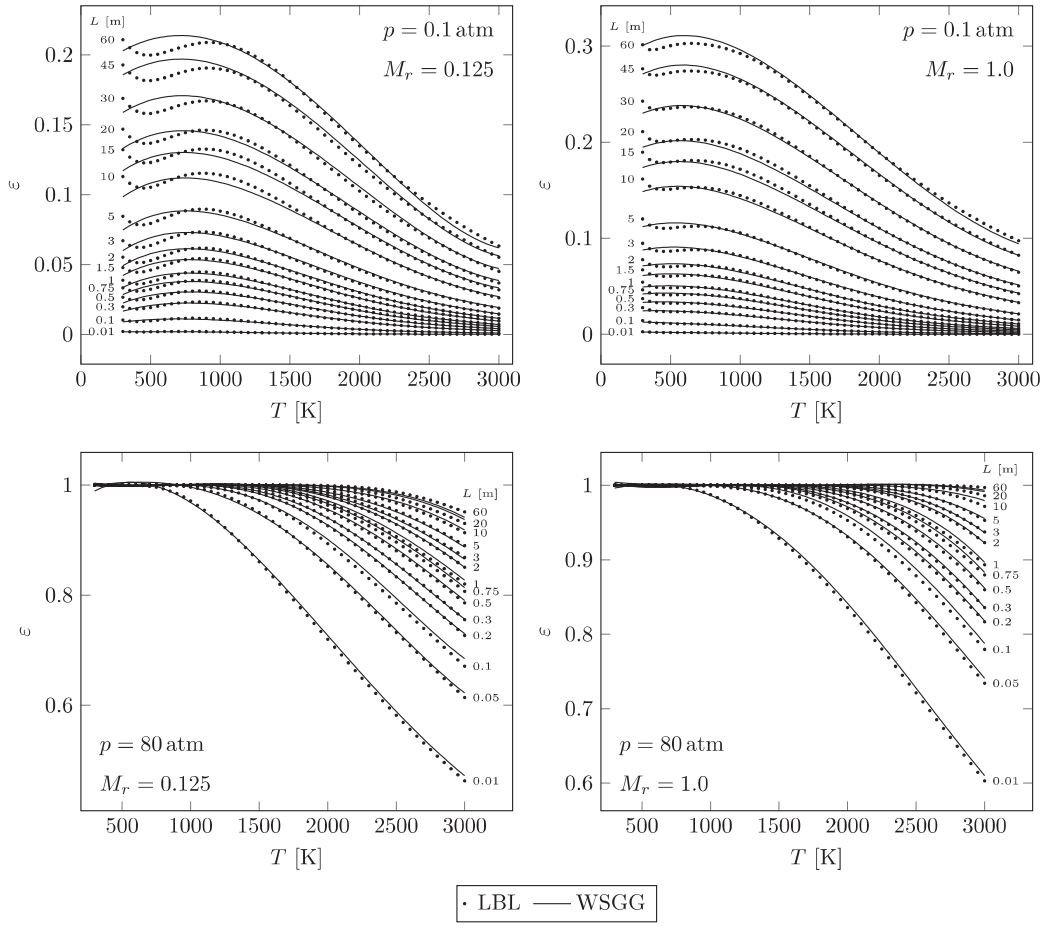

Fig. 2. Emissivity charts for typical dry and wet flue gas recycle conditions obtained by LBL integration and by the new WSGG model.

assessing the accuracy of the WSGG model is provided by the LBL integration of Eq. (12), which is also solved using the DOM with the same discretization parameters. More details on how the LBL solution is obtained may be found in [39,50,67].

Figure 3 reports the radiative heat source and radiative heat flux for Test Cases 1 to 3 for a medium at atmospheric pressure, as computed by LBL integration and by the WSGG model proposed in this paper. For comparison purposes, the results of the WSGG formulation of Shan et al. [51]—which is the only other M_r-varying WSGG correlation available in the literature that is applicable to high-pressures, cf. Table 1—are also included in the figure. Differently from the present model, the one by Ref. [51] incorporates a dependence of pressure into the gray gas weighting and absorption coefficients, but it was developed for several fixed M_r values; to account for cases with varying M_r, a stepwise approach was proposed, in a similar way to some atmospheric-pressure WSGG formulations [36,52]. The problem with this approach is that it may introduce discontinuities in the results, leading to non-physical distributions of S_r, as it will be shown later. Thus, as an attempt to circumvent this issue, an additional application of the model of Shan et al. [51] has been carried out here, where the absorption coefficient and polynomial terms that compose the weighting coefficient are linearly interpolated between their values proposed at the fixed M_r points; a similar approach has been adopted by Kez et al. [68] for testing the stepwise WSGG model of [52].

Both the new WSGG model and the one by Ref. [51] are able to capture the overall spatial behavior of S_r and q_r in Figure 3. However, while Shan's model even outperforms the present model for the prediction of the radiative heat flux in Case 1, where the mole ratio does not vary (notice that for this case the stepwise and interpolated approaches for that model yield identical results, so only the former is reported), the same is not verified for neither S_r nor q_r for Cases 2 and 3. In those cases, some abrupt changes in the spatial distribution of the radiative heat source can be observed for the application of the model of Shan et al. that uses the standard stepwise approach for determining $\kappa_{p,i}$ and a_i; these changes in the S_r slope occur precisely at points where the mole ratio transitions from one of the WSGG coefficients set in Ref. [51] to another. Similar findings [68] have been reported for other WSGG formulations that use a stepwise procedure to deal with M_r-varying scenarios. Linearly interpolating Shan's coefficients eliminates this issue, but still the accuracy of that model is less than that of the model presented in this paper.

This is further demonstrated in Table 2, that reports the maximum ("max") and medium-averaged ("avg") normalized errors for each model. The normalized error is defined as $\Delta\phi = |\phi_{\text{LBL}} - \phi_{\text{WSGG}}|/\max(|\phi_{\text{LBL}}|)$, where ϕ is either S_r or q_r; ϕ_{LBL} and ϕ_{WSGG} are the local values of ϕ obtained by the solutions with the LBL method and the WSGG model, respectively; and $\max(|\phi_{\text{LBL}}|)$ is the maximum absolute value of ϕ_{LBL} in the medium. While Shan's WSGG model shows comparable (for S_r) or smaller (for q_r) errors than the present model for Case 1, it is clear that the new model performs better for Cases 2 and 3, which correspond to varying-M_r scenarios. The improvement over the standard stepwise formulation of Shan et al. [51] is especially significant for the maximum errors, which go from ranging between 15% and 22% to, at worst, 17%. Moreover, although the maximum errors of Shan's model reduce (at least for S_r) if the interpolation approach is adopted instead, its average errors are still larger than those of the new model.

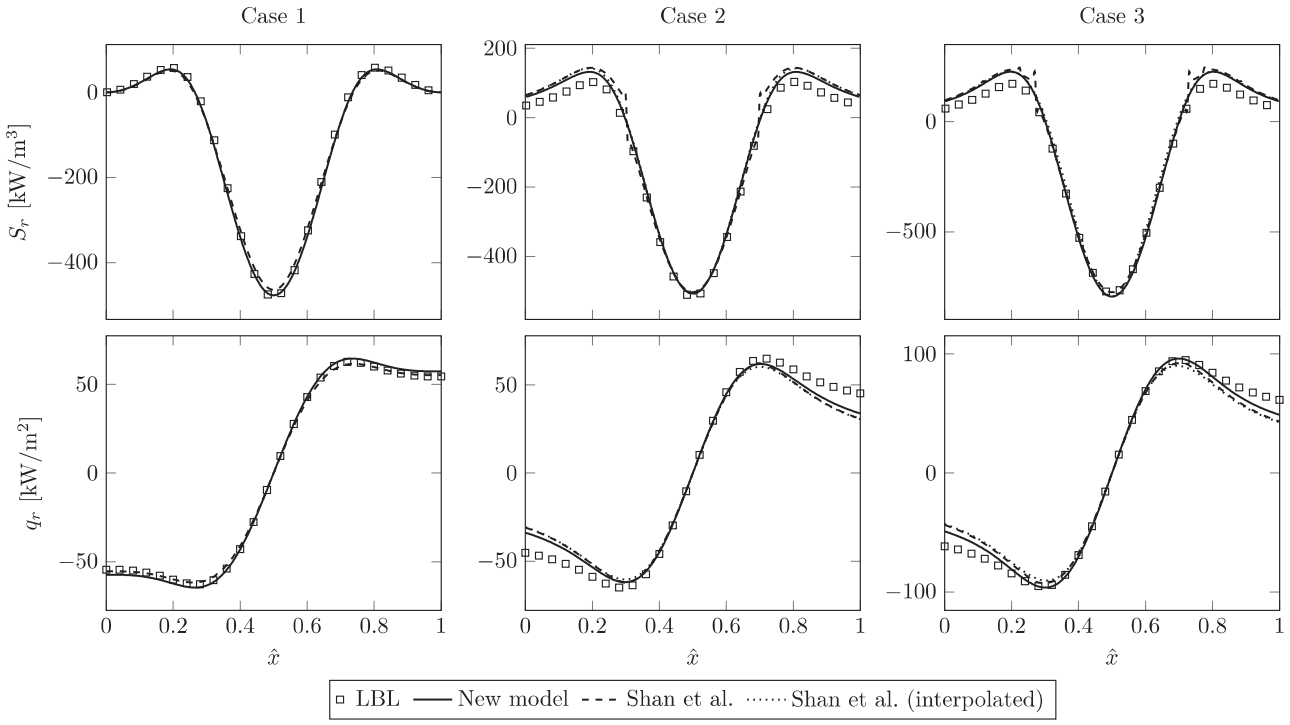

Fig. 3. Results of the test cases with $p = 1$ *atm*.

Table 2
Maximum and average (in parenthesis) normalized errors of the new model and the models of Refs. [40,51].

		New model	Bordbar et al. [40]	Shan et al. [51]	Shan et al. [51][a]
		$p = 1$ *atm*			
Case 1	ΔS_r [%]	3.09 (1.26)	3.07 (1.48)	3.44 (1.70)	–
	Δq_r [%]	4.53 (2.53)	2.63 (1.47)	3.43 (1.56)	–
Case 2	ΔS_r [%]	6.57 (4.43)	6.35 (5.41)	16.9 (5.63)	8.52 (5.60)
	Δq_r [%]	17.6 (7.29)	21.5 (10.4)	22.1 (9.34)	22.5 (9.97)
Case 3	ΔS_r [%]	7.10 (4.08)	6.83 (3.48)	15.8 (4.58)	7.44 (4.95)
	Δq_r [%]	13.2 (4.32)	14.1 (4.54)	18.9 (7.41)	19.6 (8.35)
		$p = 30$ *atm*			
Case 1	ΔS_r [%]	4.66 (1.32)	4.05 (2.18)	23.9 (6.55)	–
	Δq_r [%]	5.54 (4.14)	6.70 (4.43)	25.1 (17.6)	–
Case 2	ΔS_r [%]	6.43 (2.98)	17.3 (9.86)	59.5 (7.11)	7.44 (5.40)
	Δq_r [%]	10.0 (2.82)	18.4 (9.96)	15.0 (7.91)	14.6 (7.87)
Case 3	ΔS_r [%]	5.36 (3.04)	9.55 (4.35)	13.0 (6.31)	12.7 (5.54)
	Δq_r [%]	7.42 (3.64)	9.00 (4.97)	21.6 (12.6)	20.0 (11.9)
		$p = 0.5$ *atm*			
Case 1	ΔS_r [%]	3.30 (1.38)	5.94 (1.90)	–	–
	Δq_r [%]	5.20 (3.26)	6.79 (4.32)	–	–
Case 2	ΔS_r [%]	7.76 (4.92)	7.06 (4.21)	–	–
	Δq_r [%]	18.7 (8.08)	16.2 (5.61)	–	–
Case 3	ΔS_r [%]	7.85 (4.60)	8.76 (5.78)	–	–
	Δq_r [%]	13.9 (4.76)	8.63 (4.23)	–	–

[a] Interpolated

Table 2 includes the errors of the WSGG model of Bordbar et al. [40]. Compared to that model [40], the new model fares either as well (for Case 1) or better (for Cases 2 and 3). Particularly for Case 2, the errors of the new model are almost half of that of the older model. Nevertheless, it is interesting to note that, although it was developed for atmospheric conditions, the model of Bordbar et al. [40] has a fairly good accuracy for Case 1, even outperforming Shan's model (this is also true for Case 3).

Results for Cases 1 to 3 with a total pressure of 30 *atm* are depicted in Figure 4. For this higher pressure, the improvement in accuracy offered by the present model becomes more evident. Its errors do not surpass 10% for any of the test cases, and, on average, they are always less than 5%—for contrast, the average errors of Shan's model are, at best, above 6% (see Table 2). Furthermore, for Cases 2 and 3 (especially for the former), the non-physical spatial distribution of S_r attained with the stepwise approach of Shan's model are more clearly noticeable for $p = 30$ *atm* than for $p = 1$ *atm*, and result in local errors as high as 60%. Once again, while adopting a linear interpolation to deal with the varying mole ratio eliminates this issue, it still leads to errors considerably larger than those of the present model.

One possible reason for the overall lower performance of Shan's model could be the total pressure fitting that is performed on their correlations, which is not performed on the present model. The

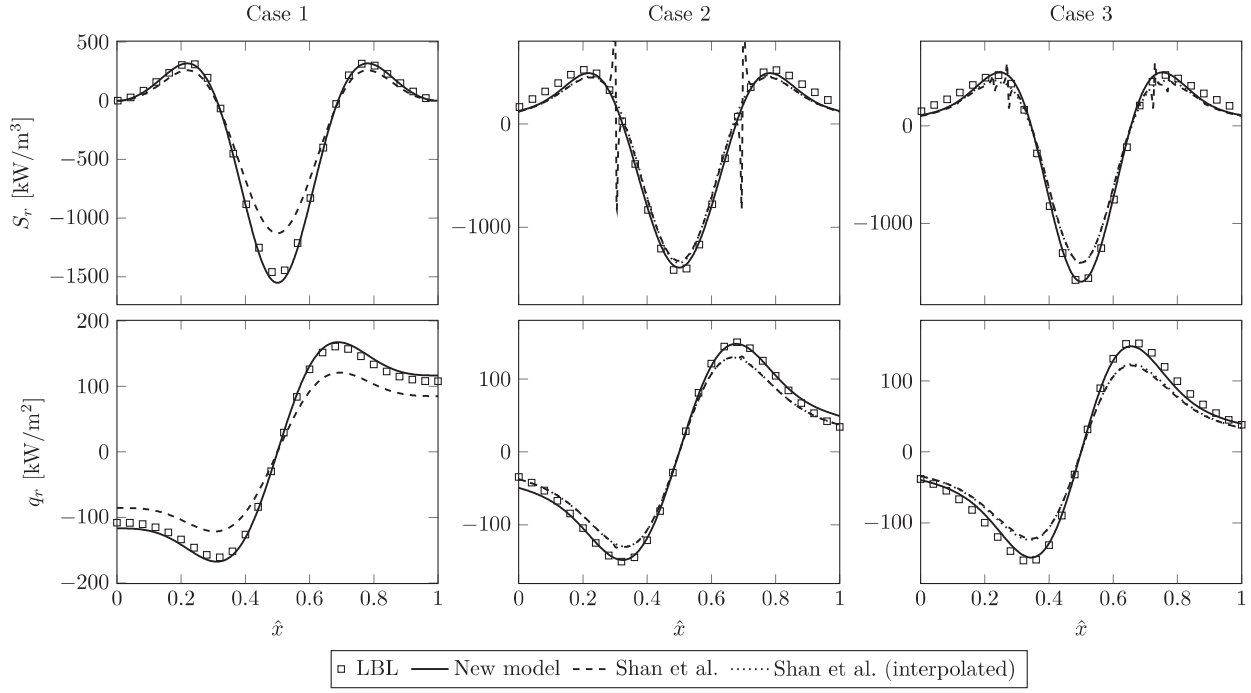

Fig. 4. Results of the test cases with $p = 30$ *atm*.

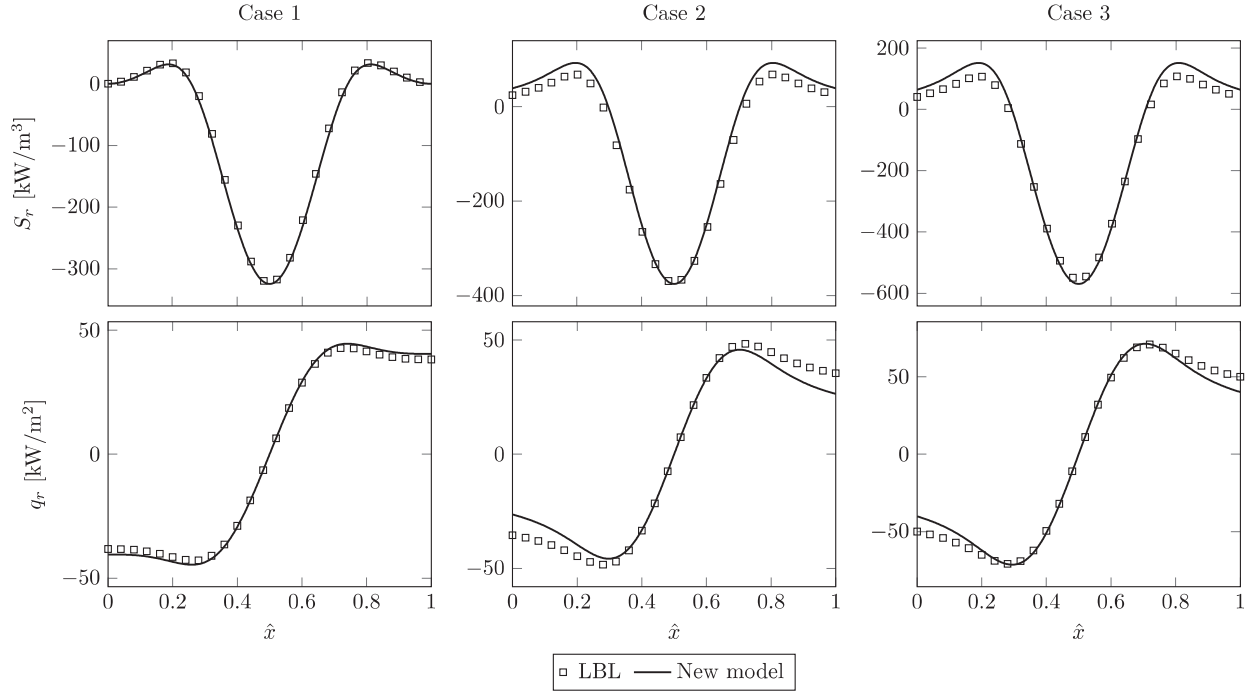

Fig. 5. Results of the test cases with $p = 0.5$ *atm*.

deviations caused by this additional fitting, even if small, might be contributing to the differences between the two models. Furthermore, Shan's coefficients are based on the EM2C narrow-band emissivities, which have their own deviations when compared to LBL emissivities. Even though the SNB usually presents great agreement with the LBL solution, the fact that the database from EM2C is based on absorption spectra that are different than the ones considered in this study might also be a relevant factor to explain the relatively lower accuracy of Shan's model.

A medium at sub-atmospheric pressure is considered next. Figure 5 plots the resulting S_r and q_r distributions for Cases 1 to 3 for a medium at a total pressure $p = 0.5$ *atm*; because no previous WSGG formulation is available for sub-atmospheric pressures, only results of the present WSGG model and of the LBL integration method are reported. For this pressure, the model performs the best for Case 1, where its average errors are below 4% for both S_r and q_r, as conveyed by Table 2. For Cases 2 and 3, the errors are larger, especially for the radiative heat flux close to the walls,

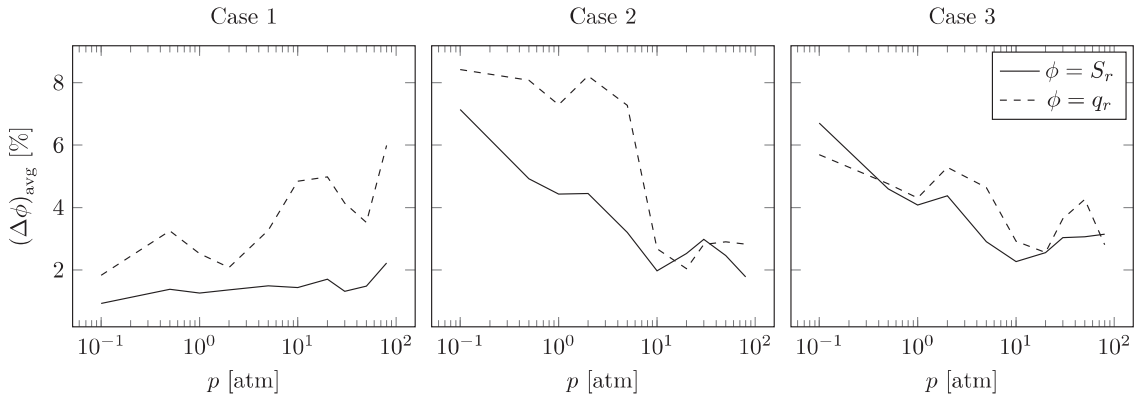

Fig. 6. Average errors in the radiative heat flux and radiative heat source for the new WSGG model as a function of the total pressure of the medium.

reaching almost 20% for Case 2. Nonetheless, on average, for the $p = 0.5$ *atm* cases the errors of the new model range between 5% and 8%.

4.3. Performance of the model across its pressure range

To further assess the performance of the new model, the temperature and species concentration profiles corresponding to Cases 1 to 3 have been simulated for different total pressures of the medium. The values chosen for p correspond to the discrete values for which the set of new WSGG correlations were developed, as discussed in Section 2, and range from 0.1*atm to* 80 *atm*.

Figure 6 reports the medium-averaged errors of the model for S_r and q_r as a function of the total pressure. Starting at $p = 10$ *atm*, the accuracy of the model does not vary much with increasing pressures, with the average errors never surpassing 5% (the exception being in the radiative heat flux for Case 1, where the average error about 6% for $p = 80$ *atm*). For sub-atmospheric pressures, the model also fares well, although for Case 2 $(\Delta q_r)_{\text{avg}}$ reaches 9.5% for $p < 1.0$ *atm*. Note that the main difference between these three cases are in how the molar fraction ratio of H_2O to CO_2 (i.e. M_r) varies along the length of the 1D benchmarks. In case 1, the M_r does not vary and always equals two. This makes the accuracy of the WSGG model better in case 1 than the other two cases in which M_r varies and therefore the inaccuracy of the WSGG model is more due to the second stage fitting over M_r, i.e. Eq. (11). The accuracy improvement seen in case 2 and 3 with increasing the pressure is guesstimated to be because of the smoother absorption spectra of the gas mixtures at high pressures. Due to simpler form of absorption spectra, the WSGG seems to better simulate the spectral radiation of the gas mixtures at higher pressures.

5. Conclusions

While recent line-by-line based WSGG models such as [40] and [38] show promising computational performance in modeling spectral radiation in large scale atmospheric combustors [22,68], their accuracy is considerably lower when they are used for modeling non-atmospheric combustion systems [21]. With this in mind, a new WSGG model was developed in the present paper for the treatment of H_2O-CO_2 mixtures with varying mole fraction ratio, applicable to temperatures between 300K and 3000 K and to total pressures of 0.1 *atm to* 80 *atm*. The model was constructed by fitting total emissivity data to the high-resolution spectral database HITEMP2010; a very good agreement was found when comparing the emissivity charts resulting from the model to those computed by line-by-line integration of the absorption spectrum. The performance of the new model was further analyzed by applying it to several one-dimensional benchmarks representing various levels of complexity in temperature and gas composition profiles. Once again, the model consistently showed a satisfactory agreement with the predictions of LBL calculations, even outperforming the only existing WSGG model applicable to the conditions studied in this work [51]. In summary, the average error in the radiative source calculated by the new model at various pressures was always less than 5%, and the worst error in the radiative heat flux was about 10%.

Declaration of Competing Interest

Reffering to manuscript entitled as “Pressure-dependent weighted-sum-of-gray-gases models for heterogeneous CO2-H2O mixtures at sub- and super-atmospheric pressure”, we wish to confirm that there are no known conflicts of interest associated with this publication and there has been no significant financial support for this work that could have influenced its outcome. We confirm that the manuscript has been read and approved by all named authors and that there are no other persons who satisfied the criteria for authorship but are not listed. We further confirm that the order of authors listed in the manuscript has been approved by all of us. We confirm that we have given due consideration to the protection of intellectual property associated with this work and that there are no impediments to publication, including the timing of publication, with respect to intellectual property. In so doing we confirm that we have followed the regulations of our institutions concerning intellectual property. We understand that the Corresponding Author is the sole contact for the Editorial process (including Editorial Manager and direct communications with the office). He is responsible for communicating with the other authors about progress, submissions of revisions and final approval of proofs. We confirm that we have provided a current, correct email address which is accessible by the Corresponding Author.

CRediT authorship contribution statement

Hadi Bordbar: Conceptualization, Methodology, Writing - original draft, Software, Validation, Formal analysis, Writing - review & editing. **Felipe R. Coelho:** Writing - review & editing, Visualization, Software, Validation, Formal analysis. **Guilherme C. Fraga:** Writing - original draft, Visualization, Software, Validation, Formal analysis. **Francis H.R. França:** Writing - review & editing, Funding acquisition. **Simo Hostikka:** Writing - review & editing, Funding acquisition.

Acknowledgments

Authors Hadi Bordbar and Simo Hostikka greatly acknowledge the support of the Academy of Finland under grant no. 314487. Author Guilherme C. Fraga thanks CNPq for his doctorate scholarship. In addition, this study was financed in part by the Coordenao de Aperfeioamento de Pessoal de Nvel Superior - Brasil (CAPES) - Finance Code 001.

Supplementary material

Supplementary material associated with this article can be found, in the online version, at doi:10.1016/j.ijheatmasstransfer.2021.121207.

References

[1] Y.M. Seo, K. Luo, M.Y. Ha, Y.G. Park, Direct numerical simulation and artificial neural network modeling of heat transfer characteristics on natural convection with a sinusoidal cylinder in a long rectangular enclosure, International Journal of Heat and Mass Transfer 152 (2020) 119564, doi:10.1016/j.ijheatmasstransfer.2020.119564.

[2] M.H. Bordbar, T. Hyppänen, Multiscale numerical simulation of radiation heat transfer in participating media, Heat Transfer Engineering 34 (1) (2013) 54–69, doi:10.1080/01457632.2013.695210.

[3] M. Darbandi, A. Fatin, H. Bordbar, Numerical study on nox reduction in a large-scale heavy fuel oil-fired boiler using suitable burner adjustments, Energy (2020) 117371, doi:10.1016/j.energy.2020.117371.

[4] M.H. Bordbar, P. Zamankhan, Dynamical states of bubbling in vertically vibrated granular materials. part i: Collective processes, Communications in Nonlinear Science and Numerical Simulation 12 (3) (2007) 254–272, doi:10.1016/j.cnsns.2005.04.001.

[5] M.H. Bordbar, T. Hyppänen, Simulation of bubble formation and heaping in a vibrating granular bed, Chemical Engineering Communications 198 (7) (2011) 905–919, doi:10.1080/00986445.2011.545295.

[6] M.H. Bordbar, P. Zamankhan, Dynamical states of bubbling in vertical vibrated granular materials. part ii: Theoretical analysis and simulations, Communications in Nonlinear Science and Numerical Simulation 12 (3) (2007) 273–299, doi:10.1016/j.cnsns.2005.03.008.

[7] M. Darbandi, M. Ghafourizadeh, Solving turbulent diffusion flame in cylindrical frame applying an improved advective kinetics scheme, Theoretical and Computational Fluid Dynamics 29 (5) (2015) 413–431.

[8] M. Darbandi, M. Ghafourizadeh, Extending a low-order upwind-biased scheme to solve turbulent flames using detailed chemistry model, Numerical Heat Transfer, Part B: Fundamentals 73 (6) (2018) 343–362, doi:10.1080/10407790.2018.1493851.

[9] M. Darbandi, B. Abrar, Advances in non-gray radiation calculation in combusting environments using a modified reference approach, Heat and Mass Transfer 54 (9) (2018) 2705–2713.

[10] H. Bordbar, T. Hyppänen, Line by line based band identification for non-gray gas modeling with a banded approach, International Journal of Heat and Mass Transfer 127 (2018) 870–884, doi:10.1016/j.ijheatmasstransfer.2018.06.093.

[11] H. Bordbar, A. Maximov, T. Hyppänen, Improved banded method for spectral thermal radiation in participating media with spectrally dependent wall emittance, Applied Energy 235 (2019) 1090–1105, doi:10.1016/j.apenergy.2018.11.033.

[12] C.A. Hoerlle, F.H.R. Frana, P.R. Pagot, F.M. Pereira, Effects of radiation modeling on non-premixed sooting flames simulations under oxyfuel conditions, Combustion and Flame 217 (2020) 294–305, doi:10.1016/j.combustflame.2020.04.012.

[13] Z. He, C. Dong, D. Liang, J. Mao, A weighted-sum-of-gray soot-fractal-aggregates model for nongray heat radiation in the high temperature gas-soot mixture, Journal of Quantitative Spectroscopy and Radiative Transfer 260 (2021) 107431, doi:10.1016/j.jqsrt.2020.107431.

[14] M.F. Modest, Radiative Heat Transfer, 3rd, Academic Press, 2013.

[15] Y.-Y. Feng, C.-H. Wang, Discontinuous finite element method applied to transient pure and coupled radiative heat transfer, International Communications in Heat and Mass Transfer 122 (2021) 105156, doi:10.1016/j.icheatmasstransfer.2021.105156.

[16] J.R. Howell, M.P. Mengüç, R. Siegel, Thermal Radiation Heat Transfer, 6th, CRC press, 2016.

[17] A. Wang, M.F. Modest, Importance of combined Lorentz-Doppler broadening in high-temperature radiative heat transfer applications, Journal of Heat Transfer 126 (5) (2004) 858–861, doi:10.1115/1.1798951.

[18] M.F. Modest, D.C. Haworth, Radiative Heat Transfer in Turbulent Combustion Systems: Theory and Applications, Springer, 2016.

[19] W. Malkmus, Random Lorentz band model with exponential-tailed S^{-1} line-intensity distribution function, Journal of the Optical Society of America 57 (3) (1967) 323, doi:10.1364/josa.57.000323.

[20] A. Soufiani, J. Taine, High temperature gas radiative property parameters of statistical narrow-band model for H_2O, CO_2 and CO, and correlated-k model for H_2O and CO_2, International Journal of Heat and Mass Transfer 40 (4) (1997) 987–991, doi:10.1016/0017-9310(96)00129-9.

[21] H. Chu, M. Gu, J.-L. Consalvi, F. Liu, H. Zhou, Effects of total pressure on nongrey gas radiation transfer in oxy-fuel combustion using the LBL, SNB, SNBCK, WSGG, and FSCK methods, Journal of Quantitative Spectroscopy and Radiative Transfer 172 (2016) 24–35, doi:10.1016/j.jqsrt.2015.07.009.

[22] V. Kez, F. Liu, J. Consalvi, J. Strhle, B. Epple, A comprehensive evaluation of different radiation models in a gas turbine combustor under conditions of oxy-fuel combustion with dry recycle, Journal of Quantitative Spectroscopy and Radiative Transfer 172 (2016) 121–133, doi:10.1016/j.jqsrt.2015.11.002.

[23] H. Chu, J.-L. Consalvi, M. Gu, F. Liu, Calculations of radiative heat transfer in an axisymmetric jet diffusion flame at elevated pressures using different gas radiation models, Journal of Quantitative Spectroscopy and Radiative Transfer 197 (2017) 12–25, doi:10.1016/j.jqsrt.2017.02.008.

[24] H. Chu, F. Ren, Y. Feng, M. Gu, S. Zheng, A comprehensive evaluation of the non gray gas thermal radiation using the line-by-line model in one- and two-dimensional enclosures, Applied Thermal Engineering 124 (2017) 362–370, doi:10.1016/j.applthermaleng.2017.06.037.

[25] A. Wang, M.F. Modest, High-accuracy, compact database of narrow-band k-distributions for water vapor and carbon dioxide, Journal of Quantitative Spectroscopy and Radiative Transfer 93 (1-3) (2005) 245–261, doi:10.1016/j.jqsrt.2004.08.024.

[26] G. Pal, M.F. Modest, k-distribution methods for radiation calculations in high-pressure combustion, Journal of Thermophysics and Heat Transfer 27 (3) (2013) 584–587, doi:10.2514/1.t3957.

[27] X. Yang, A. Clements, J. Szuhánszki, X. Huang, O.F. Moguel, J. Li, J. Gibbins, Z. Liu, C. Zheng, D. Ingham, L. Ma, B. Nimmo, M. Pourkashanian, Prediction of the radiative heat transfer in small and large scale oxy-coal furnaces, Applied Energy 211 (2018) 523–537, doi:10.1016/j.apenergy.2017.11.070.

[28] V. Kez, J.-L. Consalvi, F. Liu, T. Gronarz, J. Strhle, R. Kneer, B. Epple, Investigation of gas and particle radiation modelling in wet oxy-coal combustion atmospheres, International Journal of Heat and Mass Transfer 133 (2019) 1026–1040, doi:10.1016/j.ijheatmasstransfer.2019.01.013.

[29] Y. Liu, G. Liu, F. Liu, J-L. Consalvi, Effects of the k-value solution schemes on radiation heat transfer modelling in oxy-fuel flames using the full-spectrum correlated k-distribution method, Applied Thermal Engineering (2020) 114986, doi:10.1016/j.applthermaleng.2020.114986.

[30] J. Cai, M.F. Modest, Improved full-spectrum k-distribution implementation for inhomogeneous media using a narrow-band database, Journal of Quantitative Spectroscopy and Radiative Transfer 141 (2014) 65–72, doi:10.1016/j.jqsrt.2014.02.028.

[31] M.K. Denison, B.W. Webb, A spectral line-based weighted-sum-of-gray-gases model for arbitrary rte solvers, Journal of Heat Transfer 115 (4) (1993) 1004–1012, doi:10.1115/1.2911354.

[32] M. Denison, B.W. Webb, An absorption-line blackbody distribution function for efficient calculation of total gas radiative transfer, Journal of Quantitative Spectroscopy and Radiative Transfer 50 (5) (1993) 499–510, doi:10.1016/0022-4073(93)90043-h.

[33] J.T. Pearson, B.W. Webb, V.P. Solovjov, J. Ma, Effect of total pressure on the absorption line blackbody distribution function and radiative transfer in H_2O, CO_2, and CO, Journal of Quantitative Spectroscopy and Radiative Transfer 143 (2014) 100–110, doi:10.1016/j.jqsrt.2013.08.011.

[34] J.T. Pearson, B.W. Webb, V.P. Solovjov, J. Ma, Efficient representation of the absorption line blackbody distribution function for H_2O, CO_2, and CO at variable temperature, mole fraction, and total pressure, Journal of Quantitative Spectroscopy and Radiative Transfer 138 (2014) 82–96, doi:10.1016/j.jqsrt.2014.01.019.

[35] B. Wang, Y. Xuan, An improved WSGG model for exhaust gases of aero engines within broader ranges of temperature and pressure variations, International Journal of Heat and Mass Transfer 136 (2019) 1299–1310, doi:10.1016/j.ijheatmasstransfer.2019.03.105.

[36] C. Yin, L.C.R. Johansen, L.A. Rosendahl, S.K. Kær, New weighted sum of gray gases model applicable to computational fluid dynamics (CFD) modeling of oxy-fuel combustion: Derivation, validation, and implementation, Energy & Fuels 24 (12) (2010) 6275–6282, doi:10.1021/ef101211p.

[37] R. Johansson, B. Leckner, K. Andersson, F. Johnsson, Account for variations in the H_2O to CO_2 molar ratio when modelling gaseous radiative heat transfer with the weighted-sum-of-grey-gases model, Combustion and Flame 158 (5) (2011) 893–901, doi:10.1016/j.combustflame.2011.02.001.

[38] T. Kangwanpongpan, F.H.R. França, R.C. da Silva, P.S. Schneider, H.J. Krautz, New correlations for the weighted-sum-of-gray-gases model in oxy-fuel conditions based on HITEMP 2010 database, International Journal of Heat and Mass Transfer 55 (25) (2012) 7419–7433, doi:10.1016/j.ijheatmasstransfer.2012.07.032.

[39] L.J. Dorigon, G. Duciak, R. Brittes, F. Cassol, M. Galarça, F.H.R. França, WSGG correlations based on HITEMP2010 for computation of thermal radiation in non-isothermal, non-homogeneous H_2O/CO_2 mixtures, International Journal of Heat and Mass Transfer 64 (2013) 863–873, doi:10.1016/j.ijheatmasstransfer.2013.05.010.

[40] M.H. Bordbar, G. Wecel, T. Hyppänen, A line by line based weighted sum of gray gases model for inhomogeneous CO_2-H_2O mixture in oxy-fired combustion, Combustion and Flame 161 (9) (2014) 2435–2445, doi:10.1016/j.combustflame.2014.03.013.

[41] T. Kangwanpongpan, R.C. Da Silva, H.J. Krautz, Prediction of oxy-coal combustion through an optimized weighted sum of gray gases model, Energy 41 (1) (2012) 244–251, doi:10.1016/j.energy.2011.06.010.

[42] F.R. Centeno, F. Cassol, H.A. Vielmo, F.H.R. França, C.V. Silva, Comparison of different WSGG correlations in the computation of thermal radiation in a 2d axisymmetric turbulent non-premixed methane–air flame, Journal of the Brazilian Society of Mechanical Sciences and Engineering 35 (4) (2013) 419–430, doi:10.1007/s40430-013-0040-z.
[43] F.R. Centeno, R. Brittes, F.H.R. França, O.A. Ezekoye, Evaluation of gas radiation heat transfer in a 2D axisymmetric geometry using the line-by-line integration and WSGG models, Journal of Quantitative Spectroscopy and Radiative Transfer 156 (2015) 1–11, doi:10.1016/j.jqsrt.2015.01.015.
[44] R.J.C. Fonseca, G.C. Fraga, R.B. da Silva, F.H.R. França, Application of the WSGG model to solve the radiative transfer in gaseous systems with nongray boundaries, Journal of Heat Transfer 140 (5) (2018) 052701, doi:10.1115/1.4038548.
[45] M. Bahador, B. Sunden, Evaluation of Weighted Sum of Grey Gases Coefficients for Combustion Gases Using Predicted Emissivities From High Resolution Spectroscopic Databases, in: Proceedings of ASME Turbo Expo 2008: Power for Land, Sea and Air, ASME, 2008, pp. 1791–1799, doi:10.1115/GT2008-51028.
[46] L.S. Rothman, R.B. Wattson, R. Gamache, J.W. Schroeder, A. McCann, HITRAN HAWKS and HITEMP: high-temperature molecular database, in: J.C. Dainty (Ed.), Atmospheric Propagation and Remote Sensing IV, SPIE, 1995, pp. 105–111, doi:10.1117/12.211919.
[47] S. Tashkun, V. Perevalov, J.-L. Teffo, A. Bykov, N. Lavrentieva, CDSD-1000, the high-temperature carbon dioxide spectroscopic databank, Journal of Quantitative Spectroscopy and Radiative Transfer 82 (1-4) (2003) 165–196, doi:10.1016/s0022-4073(03)00152-3.
[48] L. Rothman, I. Gordon, R. Barber, H. Dothe, R. Gamache, A. Goldman, V. Perevalov, S. Tashkun, J. Tennyson, HITEMP, the high-temperature molecular spectroscopic database, Journal of Quantitative Spectroscopy and Radiative Transfer 111 (15) (2010) 2139–2150, doi:10.1016/j.jqsrt.2010.05.001.
[49] F.R. Coelho, F.H.R. França, WSGG correlations for H_2O and CO_2 in high pressure conditions, Procceedings of the 24th ABCM International Congress of Mechanical Engineering, ABCM, Curitiba, PR, Brazil, 2017, doi:10.26678/ABCM.COBEM2017.COB17-1025.
[50] F.R. Coelho, F.H.R. França, WSGG correlations based on HITEMP2010 for gas mixtures of H_2O and CO_2 in high total pressure conditions, International Journal of Heat and Mass Transfer 127 (2018) 105–114, doi:10.1016/j.ijheatmasstransfer.2018.07.075.
[51] S. Shan, B. Qian, Z. Zhou, Z. Wang, K. Cen, New pressurized wsgg model and the effect of pressure on the radiation heat transfer of H_2O/CO_2 gas mixtures, International Journal of Heat and Mass Transfer 121 (2018) 999–1010, doi:10.1016/j.ijheatmasstransfer.2018.01.079.
[52] C. Yin, Refined weighted sum of gray gases model for air-fuel combustion and its impacts, Energy and Fuels 27 (10) (2013) 6287–6294, doi:10.1021/ef401503r.
[53] Y. Nakamura, N. Yoshimura, T. Matsumura, H. Ito, O. Fujita, Flame spread over polymer-insulated wire in sub-atmospheric pressure: Similarity to microgravity phenomena, in: Progress in Scale Modeling, Springer Netherlands, 2008, pp. 17–27, doi:10.1007/978-1-4020-8682-3_2.
[54] N. Panek, M.R.J. Charest, O.L. Gulder, Simulation of microgravity diffusion flames using sub-atmospheric pressures, AIAA Journal 50 (4) (2012) 976–980, doi:10.2514/1.j051306.
[55] T. Yamazaki, T. Matsuoka, Y. Li, Y. Nakamura, Applicability of a low-pressure environment to investigate smoldering behavior under microgravity, Fire Technology 56 (1) (2019) 209–228, doi:10.1007/s10694-019-00911-y.
[56] J. Humleek, Optimized computation of the voigt and complex probability functions, Journal of Quantitative Spectroscopy and Radiative Transfer 27 (4) (1982) 437–444, doi:10.1016/0022-4073(82)90078-4.
[57] A. Ziemniczak, F.R. Coelho, F.M. Pereira, P.R. Pagot, F.H.R. Frana, Evaluation of the discretization in the spectral resolution for the solution of the line-by-line method in problems with participating gases, Journal of the Brazilian Society of Mechanical Sciences and Engineering 41 (9) (2019) 354.
[58] H. Chu, F. Liu, H. Zhou, Calculations of gas thermal radiation transfer in one-dimensional planar enclosure using LBL and SNB models, International Journal of Heat and Mass Transfer 54 (21) (2011) 4736–4745, doi:10.1016/j.ijheatmasstransfer.2011.06.002.
[59] X. Yang, Z. He, S. Dong, H. Tan, Evaluation of the non-gray weighted sum of gray gases models for radiative heat transfer in realistic non-isothermal and non-homogeneous flames using decoupled and coupled calculations, International Journal of Heat and Mass Transfer 134 (2019) 226–236, doi:10.1016/j.ijheatmasstransfer.2019.01.038.
[60] M.F. Modest, The weighted-sum-of-gray-gases model for arbitrary solution methods in radiative transfer, Journal of heat transfer 113 (3) (1991) 650–656, doi:10.1115/1.2910614.
[61] MATLAB Help solve nonlinear curve-fitting (data-fitting) problems in least-squares sense, (https://www.mathworks.com/help/optim/ug/lsqcurvefit.html). Accessed: 2020-04-21.
[62] B.G. Carlson, K.D. Lathrop, Transport theory - the method of discrete ordinates, in: H. Greenspan, C.N. Kelber, O. D (Eds.), Computing methods in reactor physics, Gordon and Breach, New York, 1968, pp. 165–266.
[63] W.A. Fiveland, Discrete-ordinates solutions of the radiative transport equation for rectangular enclosures, Journal of Heat Transfer 106 (4) (1984) 699–706, doi:10.1115/1.3246741.
[64] M.M. Galarça, A. Mossi, F.H.R. França, A modification of the cumulative wavenumber method to compute the radiative heat flux in non-uniform media, Journal of Quantitative Spectroscopy and Radiative Transfer 112 (3) (2011) 384–393, doi:10.1016/j.jqsrt.2010.09.007.
[65] K.D. Lathrop, B.G. Carlson, Discrete Ordinates Angular Quadrature of the Neutron Transport Equation, Technical Report, 1964, doi:10.2172/4666281.
[66] ANSYS Fluent User's Guide, ANSYS, Inc., release 17.2. edition, 2016.
[67] F. Cassol, R. Brittes, F.H.R. França, O.A. Ezekoye, Application of the weighted-sum-of-gray-gases model for media composed of arbitrary concentrations of H_2O, CO_2 and soot, International Journal of Heat and Mass Transfer 79 (2014) 796–806, doi:10.1016/j.ijheatmasstransfer.2014.08.032.
[68] V. Kez, J. Consalvi, F. Liu, J. Strhle, B. Epple, Assessment of several gas radiation models for radiative heat transfer calculations in a three-dimensional oxy-fuel furnace under coal-fired conditions, International Journal of Thermal Sciences 120 (2017) 289–302, doi:10.1016/j.ijthermalsci.2017.06.017.